PHYSICAL REVIEW D **78,** 124016 (2008)

Stability of self-gravitating accreting flows

Patryk Mach[1] and Edward Malec[1,2]

[1]*M. Smoluchowski Institute of Physics, Jagiellonian University, Reymonta 4, 30-059 Kraków, Poland*

[2]*Physics Department, UCC, Cork, Ireland*

(Received 24 October 2008; published 18 December 2008)

Analytic methods show stability of the stationary accretion of test fluids but they are inconclusive in the case of self-gravitating stationary flows. We investigate numerically stability of those stationary flows onto compact objects that are trans-sonic and rich in gas. In all studied examples solutions appear stable. Numerical investigation suggests also that the analogy between sonic and event horizons holds for small perturbations of compact support but fails in the case of finite perturbations.

DOI: 10.1103/PhysRevD.78.124016 PACS numbers: 04.40.Nr, 95.30.Lz, 95.30.Sf

I. INTRODUCTION

Investigation of the spherical accretion onto compact objects starts with seminal works of Hoyle, Lyttleton, and Bondi [1–3] describing the infall of dust matter onto a surface of a star moving through the interstellar medium. The first hydrodynamical analysis of spherical accretion was presented in 1952 by Bondi [4] who considered a spherically symmetric flow of a polytropic perfect fluid in a Keplerian gravitational potential. A general-relativistic model of accretion in the Schwarzschild space-time has been developed by Michel [5]. In all these works the test fluid approximation has been adopted.

The first general-relativistic model with self-gravitating steady fluids has been analyzed by Malec [6]. This work has been later continued by Karkowski, Kinasiewicz, Mach, Malec, and Świerczyński [7], and resulted in finding a whole family of steady trans-sonic solutions of Einstein equations describing a self-gravitating cloud of gas accreting onto a central compact object (a black hole in this particular case). The most striking fact about these solutions is that, given fixed asymptotic parameters of the model (such as the size of the cloud, speed of sound at the outer boundary, and the total asymptotic mass of the system), there exist two different trans-sonic solutions corresponding to the same accretion rate—one, for which most of the mass is contained in the central object, and the other, where the amount of mass contained in the accreting fluid constitutes almost all the mass of the entire configuration. The first class of the solutions contains a subset of the test fluid flows found by Michel. Other solutions are new. Let us stress that, although these solutions are not available in a closed form, many of their parameters and properties can be inferred by analytical means. Such flows might be associated with the Thorne-Żytkow stars [8,9] or quasistars [10].

We should also mention here the work of Papadopoulos and Font [11], who constructed a general-relativistic hydrodynamical code capable of simulating self-gravitating flows and applied it to the strongly perturbed Michel's solution. The fluid perturbation was treated as self-gravitating but the background solution corresponded to the test fluid regime. A similar investigation, but in the context of radiation hydrodynamics, has been done by Zampieri *et al.* [12]. They investigated the stability of solutions in Schwarzschild space-time found by Nobili *et al.* [13].

The first proof of the stability of the trans-sonic accretion in the Newtonian and relativistic, spherically symmetric cases, given by Moncrief [14], was restricted to the test fluid approximation. Analytic methods are inconclusive in the case of self-gravitating accretion flows [15]. Below we report the results of a numerical analysis of the stability of both branches of solutions found in [7]. An interesting by-product of this investigation is that in the nonlinear regime sonic horizons are movable and the signal can get out from within the sonic horizon in the original steady flow. That hints to the limited validity of the formal analogy between sonic and event horizons.

A stability analysis of Newtonian accretion solutions with self-gravitating flows has been done for axially symmetric perturbations. In all examined cases we have observed the stable behavior of both aforementioned branches of solutions: those corresponding to the test fluid as well as those where the mass of the fluid dominates over the mass of a central object.

The order of the forthcoming sections is as follows. Section II gives a short description of the two branches of accreting flows in spherically symmetric space-times. Section III introduces the dynamical equations of motion in the form adopted in the numerical code. Section VI reports results concerning stability of accreting flows. The next section shows that sonic horizons can be penetrated from within by large perturbations. This suggests the limited validity of the analogy between sonic and event horizons. The stability of Newtonian accretion under axisymmetric perturbations is shown in Sec. VIII. Obtained results are briefly reviewed in Sec. VIII.

II. STEADY SOLUTIONS

A general spherically symmetric space-time can be described by the line element,

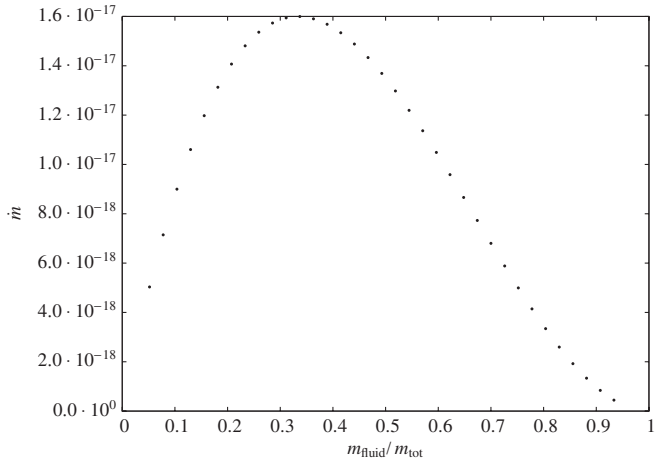

FIG. 1. The dependence of the accretion rate $\dot{m}$ on the m_{fluid}. Here $m_{\mathrm{tot}} = 1$.

$$ds^2 = -N^2 d\tilde{t}^2 + \alpha dr^2 + R^2(d\theta^2 + \sin^2\theta d\phi^2), \qquad (1)$$

where N, α, and R are functions of the coordinate radius r and the asymptotic time variable $\tilde{t}$.

The extrinsic curvature of a slice of constant time $\tilde{t}$ of the space-time with the metric given by (1) has the following nonzero elements: $K^r_r = \partial_{\tilde{t}}\alpha/(2\alpha N)$, $K^\theta_\theta = K^\phi_\phi = \partial_{\tilde{t}} R/(RN)$. Accordingly the trace of the extrinsic curvature can be written as $\mathrm{tr}K = N^{-1}\partial_{\tilde{t}} \ln(\sqrt{\alpha}R^2)$.

Similar calculations can be performed for the two-spheres of constant radius r embedded in a given temporal slice. The result for the trace of the extrinsic curvature (twice the mean curvature of the surface) is $k = 2\partial_r R/(R\sqrt{\alpha})$.

In what follows we will consider the evolution of a spherical cloud of perfect fluid accreting onto a central object and described by the energy-momentum tensor

$$T^{\mu\nu} = (p + \rho)u^\mu u^\nu + p g^{\mu\nu}, \qquad (2)$$

where p is the pressure, ρ the energy density, and u^μ the four-velocity of the fluid.

We start working with the comoving gauge, so that $u^r = u^\theta = u^\phi = 0$ (there exists a suitable geometric condition imposed on extrinsic curvatures K^j_i for such a choice of coordinates [6]), and introduce a function $U \equiv RK^\theta_\theta = \partial_{\tilde{t}} R/N$. It has the meaning of the spatial part of the fluid four-velocity computed in the reference frame (t', r') that has been obtained by the transformation $(\tilde{t}, r) \mapsto (t' = \tilde{t}, r' = R(\tilde{t}, r))$. We also introduce the quasilocal mass, which can be easily expressed as

$$m(R) = m_{\mathrm{tot}} - 4\pi \int_R^\infty R'^2 \rho dR'.$$

Here m_{tot} is the total asymptotic mass of the configuration, and R_∞ denotes the size of the accretion cloud. Another important quantity, the local speed of sound a is defined by

$$a^2 = \frac{1}{h}\left(\chi + \frac{p\kappa}{n^2}\right).$$

Symbols χ and κ are used here to denote derivatives

$$\chi = \left(\frac{\partial p}{\partial n}\right)_\epsilon, \qquad \kappa = \left(\frac{\partial p}{\partial \epsilon}\right)_n,$$

which have to be computed according to the assumed equation of state; the quantity $h = (\rho + p)/n$ is the specific enthalpy. For a barotropic equation of state the above definition reduces to $a^2 = dp/d\rho$.

We will search for the solutions of the Einstein equations according to the following notion of stationarity. The accretion rate $\dot{m} = \partial_{t'} m$, computed at a given areal radius R should be constant in time. Similarly, other hydrodynamical quantities like the fluid velocity U, pressure p, energy density ρ, etc. should satisfy $\partial_{t'} X = 0$, where $X = U, p, \rho, \ldots$. These assumptions can be satisfied only approximately as the accreting fluid contributes to the growing mass of the central object and the whole configuration must change in time. We will, however, see that they lead to solutions characterized by very small accretion rates both in the test and in the heavy fluid regime. Thus, for a very long time (much larger than a characteristic dynamical time understood as a time required by a sound wave to travel across the cloud), the motion of the accreting gas remains almost unchanged, and the above assumptions are justified *a posteriori*.

Under these assumptions the set of Einstein partial differential equations and the equations expressing the conservation of the energy-momentum tensor reduces to a set of ordinary ones, namely,

$$\frac{d}{dR}\ln\left(\frac{N}{kR}\right) = \frac{16\pi}{k^2 R}(\rho + p), \qquad U = \frac{A}{R^2 n},$$
$$N = \frac{Bn}{\rho + p}, \qquad kR = 2\sqrt{1 - \frac{2m}{R} + U^2}. \qquad (3)$$

Here A and B are integration constants. The baryonic density n is defined as a function assuring that $\nabla_\mu(nu^\mu) = 0$. When deriving these equations we have tacitly assumed that the equation of state is of a barotropic form $p = p(\rho)$ or, equivalently, $p = p(n)$. In the following we will specialize to the polytropic equation of state $p = Kn^\Gamma$.

In addition to these equations a suitable set of boundary conditions has to be specified. As such we usually choose the size of the accretion cloud R_∞, its total mass m_{tot}, the asymptotic value of the baryonic density n_∞ (alternatively ρ_∞ can be also used), and the asymptotic value of the speed of sound a_∞.

Such boundary conditions still provide a family of the solutions parametrized by the value of U_∞, or the constant A. In this work we are only interested in the so-called transsonic solutions—those for which far away from the central object the fluid is subsonic while in the central parts of the cloud it falls supersonically. Such a solution passes through

the so-called sonic point, defined as a location where $2U/(kR) = a$.

The analysis presented in [7] is concerned with accretion flows onto a central black hole which will naturally appear in the model if we continue to integrate the equations from the outer boundary inwards until the apparent horizon is passed by. In the terms of this paper the apparent horizon is defined as a surface on which the optical scalar $\theta_+ = kR/2 + U$ vanishes. According to this definition, the radius of the apparent horizon $R_{\rm BH}$ and the mass $m_{\rm BH} = m(R_{\rm BH})$ (the mass of the black hole) satisfy the standard relation $R_{\rm BH} = 2m_{\rm BH}$. Apart from the mass of the black hole we also define the fluid mass as $m_{\rm fluid} = m_{\rm tot} - m_{\rm BH}$.

Figure 1 shows the dependence of the accretion rate on the ratio of $m_{\rm fluid}/m_{\rm tot}$ for the specific case of a sequence of polytropic models with $R_\infty = 10^6$, $m_{\rm tot} = 1$ and $a_\infty = 0.1$. (The ratio of $m_{\rm fluid}/m_{\rm tot}$ scales linearly with n_∞.) Clearly, the slowly accreting regime corresponds either to a situation with a very small mass of the fluid as compared to the mass of the central black hole or to the converse case where almost the entire mass is in the form of fluid. This can actually be proved analytically [7]. Moreover, it can be shown that the maximum of $\dot{m}$ corresponds to $m_{\rm fluid}/m_{\rm tot} = 1/3$.

The attempts to investigate the stability of the new branch of massive solutions analytically have failed to give any conclusive results (see, e.g., [15]). Because of this fact we devote this paper to study this numerically.

III. DESCRIPTION OF THE NUMERICAL CODE

The dynamical code used to investigate the stability of steady solutions was constructed in a similar fashion to the one described in [16]. It is a modern version of a high resolution shock-capturing (HRSC) scheme based on the Godunov-type methods developed for solving the equations of hydrodynamics.

For the construction of the code the polar gauge has been used. The metric is assumed to be of the form

$$ds^2 = -\alpha^2 dt^2 + X^2 dR^2 + R^2(d\theta^2 + \sin^2\theta d\phi^2), \quad (4)$$

where the lapse α and X are functions of the areal radius R and time t. Following [17] we introduce the Lorentz factor $W = \alpha u^t$ and the three-velocity $v^i = u^i/W$. The equations of conservation of the energy-momentum tensor $\nabla_\mu T^{\mu\nu} = 0$ and the baryonic density $\nabla_\mu(nu^\mu) = 0$ can be now written as

$$\partial_t \mathbf{q} + \frac{1}{XR^2}\partial_R(\alpha X R^2 \mathbf{F}) = \alpha\mathbf{\Sigma} - (\partial_t \ln X)\mathbf{q}.$$

Here $\mathbf{q}$ denotes a vector of conserved quantities

$$\mathbf{q} = (D, S, \tau)^T = (nW, nhW^2 v_R, nW(hW-1) - p)^T,$$

$\mathbf{F}$ stands for the flux vector

$$\mathbf{F} = (nWv^R, nhW^2 v_R v^R + p, nW(hW-1)v^R)^T,$$

and $\mathbf{\Sigma}$ denotes the source terms

$$\mathbf{\Sigma} = \begin{pmatrix} 0 \\ (nhW^2 v_R v^R + p)\frac{\partial_R X}{X} - (nhW^2 - p)\frac{\partial_R \alpha}{\alpha} + \frac{2p}{R} \\ -nhW^2 v^R \frac{\partial_R \alpha}{\alpha} - (nhW^2 v_R v^R + p)\frac{\partial_t X}{\alpha X} \end{pmatrix}.$$

Time derivatives of conserved quantities $\mathbf{q}$ are computed according to the following version of the method of lines:

$$\left(\frac{d\mathbf{q}}{dt}\right)_i = -\frac{(\alpha X R^2 \hat{\mathbf{F}})_{i+1/2} - (\alpha X R^2 \hat{\mathbf{F}})_{i-1/2}}{X_i R_i^2 \Delta R_i} + \left(\alpha\mathbf{\Sigma} - \frac{\partial_t X}{X}\mathbf{q}\right)_i, \quad (5)$$

where lower indices refer to spatial cells (shells of constant radius). Values of $\mathbf{q}$ corresponding to the subsequent time step are obtained using standard Runge-Kutta methods.

The numerical scheme is stabilized by a suitable choice of the numerical fluxes $\hat{\mathbf{F}}_{i+1/2}$. In most of the modern HRSC schemes numerical fluxes at the cells interfaces are computed based on the solutions to the local Riemann problems that arise naturally between each of the cells' interfaces. In the following $\mathbf{q}_{{\rm L},i+1/2}$ and $\mathbf{q}_{{\rm R},i+1/2}$ will denote left and right Riemann states at the $i + 1/2$ interface. In order to provide higher order of the spatial accuracy, the states $\mathbf{q}_{{\rm L},i+1/2}$ and $\mathbf{q}_{{\rm R},i+1/2}$ are computed as follows:

$$\mathbf{q}^{\rm L}_{i+1/2} = \mathbf{q}_i + \mathbf{S}_i(R_{i+1/2} - R_i),$$
$$\mathbf{q}^{\rm R}_{i+1/2} = \mathbf{q}_{i+1} + \mathbf{S}_{i+1}(R_{i+1/2} - R_{i+1}).$$

Here R_i and $R_{i+1/2}$ are the positions of the cells' centers and interfaces, respectively. The slope limiters S_i are defined by

$$\mathbf{S}_i = \text{minmod}\left(\frac{\mathbf{q}_{i+1} - \mathbf{q}_i}{R_{i+1} - R_i}, \frac{\mathbf{q}_i - \mathbf{q}_{i-1}}{R_i - R_{i-1}}\right),$$

where the "minmod" function has been introduced as in [18]:

$$\text{minmod}\,(a, b) = \begin{cases} a & \text{if } |a| < |b|, ab > 0, \\ b & \text{if } |a| > |b|, ab > 0, \\ 0 & \text{if } ab \le 0. \end{cases}$$

As a method to compute numerical fluxes $\hat{\mathbf{F}}_{i+1/2}$, we have used two versions of a scheme proposed originally by Donat and Maraquina in [19], both of them being based on the spectral decomposition of the Jacobian $\partial\mathbf{F}/\partial\mathbf{q}$ consisting of three eigenvalues λ_p, left eigenvectors $\boldsymbol{l}p$ and right ones $\mathbf{r}_p$. In the original version of the algorithm, one starts by computing the following variables:

$$\omega^p_{\rm L} = \mathbf{l}^p_{\rm L} \cdot \mathbf{q}_{\rm L}, \qquad \omega^p_{\rm R} = \mathbf{l}^p_{\rm R} \cdot \mathbf{q}_{\rm R}$$

and

$$\phi^p_{\rm L} = \mathbf{l}^p_{\rm L} \cdot \mathbf{F}(\mathbf{q}_{\rm L}), \qquad \phi^p_{\rm R} = \mathbf{l}^p_{\rm R} \cdot \mathbf{F}(\mathbf{q}_{\rm R}),$$

where p numbers the eigenvectors of $\partial\mathbf{F}/\partial\mathbf{q}$. Now, for each p, the signs of λ^p_{L} and λ^p_{R} are inspected. If both eigenvalues λ^p_{L} and λ^p_{R} are positive, we define

$$\phi^p_+ = \phi^p_{\mathrm{L}}, \qquad \phi^p_- = 0,$$

while for both λ^p_{L} and λ^p_{R} having negative values, we set

$$\phi^p_+ = 0, \qquad \phi^p_- = \phi^p_{\mathrm{R}}.$$

If the signs of the two eigenvalues λ^p_{L} and λ^p_{R} differ, one defines $|\lambda^p|_{\max(\mathrm{L,P})} = \max(|\lambda^p_{\mathrm{L}}|, |\lambda^p_{\mathrm{R}}|)$ and

$$\phi^p_+ = \tfrac{1}{2}(\phi^p_{\mathrm{L}} + |\lambda^p|_{\max(\mathrm{L,P})}\omega^p_{\mathrm{L}}),$$
$$\phi^p_- = \tfrac{1}{2}(\phi^p_{\mathrm{R}} + |\lambda^p|_{\max(\mathrm{L,P})}\omega^p_{\mathrm{R}}).$$

The total numerical flux is now computed according to the formula

$$\hat{\mathbf{F}}_{i+1/2} = \sum_p (\phi^p_+ \mathbf{r}^p_{\mathrm{L}} + \phi^p_- \mathbf{r}^p_{\mathrm{R}}).$$

Apart from this algorithm, known in the literature as the Maraquina's flux formula, we have also implemented its slight modification described in [20]. Here the numerical fluxes are computed as

$$\hat{\mathbf{F}}_{i+1/2} = \frac{1}{2}\Big\{\mathbf{F}(\mathbf{q}_{\mathrm{L}}) + \mathbf{F}(\mathbf{q}_{\mathrm{R}}) - \sum_p |\lambda_p|_{\max(L,R)} \times ((\mathbf{l}_{p,\mathrm{R}}\cdot\mathbf{q}_{\mathrm{R}})\mathbf{r}_{p,\mathrm{R}} - (\mathbf{l}_{p,\mathrm{L}}\cdot\mathbf{q}_{\mathrm{L}})\mathbf{r}_{p,\mathrm{L}})\Big\}.$$

We have not observed any significant difference in the code performance between these two schemes.

A spectral decomposition of the Jacobian $\partial\mathbf{F}/\partial\mathbf{q}$ can be easily obtained analytically. Its eigenvalues read

$$\lambda_0 = v^R, \qquad \lambda_+ = \frac{Xv^R + a}{X + av_R}, \qquad \lambda_- = \frac{Xv^R - a}{X - av_R}.$$

Let us introduce the following quantities:

$$\mathcal{K} = \frac{\kappa}{\kappa - na^2}, \qquad \mathcal{A}_\pm = \frac{1 - v_R v^R}{1 - v_R\lambda_\pm},$$

and

$$\Delta = (\mathcal{A}_+\lambda_+ - \mathcal{A}_-\lambda_-)X^2h^3W(\mathcal{K} - 1)(1 - v_R v^R).$$

With their help the right eigenvectors of $\partial\mathbf{F}/\partial\mathbf{q}$ can be written as

$$\mathbf{r}_0 = \left(\frac{\mathcal{K}}{hW}, v_R, 1 - \frac{\mathcal{K}}{hW}\right)^T,$$

$$\mathbf{r}_\pm = (1, hWX^2\lambda_\pm\mathcal{A}_\pm, hW\mathcal{A}_\pm - 1)^T.$$

For the left eigenvectors we have

$$\mathbf{l}_0 = \frac{W}{\mathcal{K} - 1}(h - W, Wv^R, -W)^T,$$

$$\mathbf{l}_\pm = \mp\frac{h^2}{\Delta} \times \begin{pmatrix} hW\mathcal{A}_\mp(v_R - X^2\lambda_\mp) - v_R + \mathcal{K}X^2\mathcal{A}_\mp\lambda_\mp \\ 1 - \mathcal{K}\mathcal{A}_\mp, \\ -v_R + \mathcal{K}\mathcal{A}_\mp X^2\lambda_\mp \end{pmatrix}.$$

In the spherically symmetric case and the polar gauge the Einstein equations can be reduced to just two ordinary differential equations in R, that can be subsequently solved by quadratures provided that the hydrodynamical equations are known (see e.g. [21]). The first of these equations

$$\partial_R m = 4\pi R^2(nhW^2 - p) = 4\pi R^2(D + \tau)$$

gives the radial derivative of the quasilocal mass, related to the metric function X by

$$X = \frac{1}{\sqrt{1 - \frac{2m}{R}}}. \tag{6}$$

The second one provides the radial derivative of the logarithm of the lapse

$$\partial_R \ln\alpha = X^2\left(\frac{m}{R^2} + 4\pi R(nhW^2 v_R v^R + p)\right) = X^2\left(\frac{m}{R^2} + 4\pi R(Sv^R + p)\right). \tag{10}$$

These equations are integrated (numerically) at each time step, that is after new values of the hydrodynamic quantities have been obtained. Notice that the equation for mass m has to be solved before we attempt to integrate the equation for $\ln\alpha$. For a closed system, one can fix the total mass of the system and integrate the first equation starting from the outer boundary R_∞. Then the second equation can be integrated in the same way assuming, for instance, that the lapse at the outer boundary is given by the standard expression known from the Schwarzschild solution in the polar gauge:

$$\alpha(R_\infty) = \sqrt{1 - \frac{2m(R_\infty)}{R_\infty}}.$$

Let us remark, however, that such an assumption for the lapse is not necessary for the proper behavior of the hydrodynamic part of the code.

The Einstein equations yield also the following expression:

$$\partial_t X = -4\pi nh\alpha W^2 X v_R R,$$

which is required in order to establish the source terms needed by the evolution scheme (5).

Recovery of the primitive quantities (n, v^R, p) from the conserved ones (D, S, τ) is performed every time step by means of the Newton-Raphson technique (we solve an equation for the pressure p).

IV. CODE TESTS

Our numerical code has been tested on the spherical shock reflection problem [22], the Michel solution for spherical accretion in the Schwarzschild space-time [5], and models of spherical polytropic stars [23].

The first test checks the validity of the hydrodynamical part of the code in spherical symmetry. Initial data for this problem consist of a spherically symmetric flow of perfect fluid with a constant, negative radial velocity v_0. The initial baryonic density distribution is also constant and the internal energy density is set to a negligibly small value. Such initial data evolve by producing a strong shock wave appearing at $r = 0$ and propagating outward with velocity equal to

$$v_s = \frac{(\Gamma - 1)W_0|v_0|}{W_0 + 1},$$

where W_0 is the Lorentz factor corresponding to v_0.

The second test checks the validity of the implementation in a case of the test fluid accretion occurring in the fixed Schwarzschild background. The initial data for this test can be easily obtained by solving an algebraic equation for each value of the areal radius.

The initial data for the third test, namely, a static solution describing a polytropic star, have to be computed by solving the Tolman-Oppenheimer-Volkov equations for a polytropic equation of state [23]. In this case satisfactory results have been obtained using a Runge-Kutta scheme of 8th order by Hairer and Wanner [24].

All these tests have been passed as desired, convincing us that all parts of the code work properly.

V. INITIAL CONDITIONS

In order to construct the initial data for the main study of this paper, we have taken numerical, trans-sonic solutions to the equations (3) and added a perturbation in velocity. The way of obtaining such solutions is simple but not entirely obvious; we will describe it briefly here.

Instead of solving the equations in R we introduce a new independent variable $\zeta = 1/R$, which results in a grid that becomes naturally dense in the inner regions of the cloud and relatively coarse outside. Next we introduce the following set of dependent variables:

$$y_1 = \int_R^{R_\infty} dR' R'^2 \rho, \quad y_2 = 16\pi \int_R^{R_\infty} \frac{\rho + p}{k^2 R'} dR', \quad y_3 = a^2,$$

and express the equations (3) in terms of y_1, y_2, y_3, and ζ. This yields a set of three differential-algebraic equations that can be integrated starting from $\zeta_\infty = 1/R_\infty$ towards increasing values of ζ (that is from the outer boundary to the center of the cloud) provided that the values of $m_{\rm tot}$, n_∞, a_∞, and A are specified.

We solved these equations using DASPK—a solver for a system of differential and algebraic equations developed by Petzold, Brown, Hindermarsh, and Li [25,26].

Usually, the solution found in this way will not pass through the sonic point. We can, however, search for the trans-sonic solution by exploiting the fact that it can be integrated to values of ζ corresponding to the region inside the apparent horizon. (This is not true for other solutions which break down outside the horizon.) Thus, in order to find a trans-sonic flow, we have implemented a bisection method, which looks for a value of A giving the maximal ζ at which the corresponding solution crashes. After the proper value of A had been obtained, we could confirm that the appropriate solution indeed passes through the sonic point.

Such a solution is expressed in the coordinate system where the time coordinate is the comoving time. Before treating it as a possible initial data, one has to express the fluid velocity in the polar gauge. By adopting the areal radius as the radial coordinate we have changed from the comoving gauge metric given by the line element (1) to the coordinates $t'(\tilde{t}, r) = \tilde{t}$, $r'(\tilde{t}, r) = R(\tilde{t}, r)$. This leads to the line element

$$ds^2 = -\left(N^2 - \left(\frac{2}{kR}UN\right)^2\right)dt'^2 - 2UN\left(\frac{2}{kR}\right)^2 dt' dR + \left(\frac{2}{kR}\right)^2 dR^2 + R^2(d\theta^2 + \sin^2\theta d\phi^2). \tag{13}$$

Here the four-velocity of the fluid reads

$$u^{t'} = \frac{1}{N}, \qquad u^R = U, \qquad u^\theta = u^\phi = 0.$$

The transition to the polar coordinates with the metric of the form (4) can also be easily done. The function X is given by (6) and the velocity $v^R = u^R/W$—which is one of the dynamical variables in our code—can be written as

$$v^R = \frac{U}{\sqrt{1 + X^2U^2}}.$$

In this way we have obtained four functions $m(R)$, $v^R(R)$, $n(R)$, and $\epsilon(R)$ that correspond to stationary flow.

VI. STABILITY OF ACCRETING SELF-GRAVITATING FLOWS

The code described in the preceding section has been used in order to evolve perturbed steady accretion flows.

In addition to the initial data, one has to specify suitable boundary conditions. At the inner boundary outflow conditions have been assumed (the fluid was allowed to fall inward). This boundary was positioned outside the apparent horizon but always in the supersonic zone of the accretion cloud, so that the outflow conditions could be easily implemented. Thus, our numerical models resemble also a situation in which the accreting fluid is glued to the solid surface of the central body. Such an approach has been adopted for instance in [27], where the processes of the radiation transport through the accreting medium are also taken into account.

The outer boundary was kept fixed using the values obtained from the initial solution (the ghost zones were filled with the appropriate initial values). This last condition cannot be easily relaxed. After setting the outer boundary condition to an outflowing one, even the test fluid solution can be unstable.

As the first step in the stability analysis we performed a consistency check, by assuming initial data for the dynamical equations to be equal to $m(R)$, $v^R(R)$, $n(R)$, and $\epsilon(R)$ inherited from the steady flow solution. It appeared that the evolution did not produce any noticeable changes; this confirms the validity of the assumption of stationarity. Next, we introduce an additional perturbation. In our case it was applied to the velocity v^R [the other three initial data $m(R)$, $n(R)$, and $\epsilon(R)$ are the same as in the steady flow]; v^R was perturbed by a bell-shape profile of a sine wave restricted to one-half of its period. Such perturbation, initially located outside the sonic radius, produces two signals: one traveling outwards and one towards the center. If the initial amplitude of the perturbation is very small and its support is relatively narrow, the signal propagating inwards passes through the sonic point and eventually disappears through the inner boundary (it falls onto the central body).

Figure 2 shows the evolution of tiny perturbations of compact support. Here, in order to visualize any changes, we were forced to plot the contrast of density, i.e., $(n - n_0)/n_0$, where n_0 refers to the unperturbed flow. In our case this value is of order 10^{-6}, demonstrating the quality of the method by being able to handle solutions up to such precision. This, however, requires some fine-tuning in the postprocessing of the data. It is, for instance, well known that the very process of interpolating the initial solution onto a new grid introduces small numerical errors, which can easily be observed at high precision. Thus, in order to eliminate such effects, we have evolved the unperturbed flow to get the values of n_0 used to calculate the density contrast at different times.

The background solution used in this example corresponded to the following parameters: The exponent in the polytropic equation of state was set to $\Gamma = 1.4$, the asymptotic mass of the whole configuration has been normalized to unity, the outer boundary of the cloud was placed at $R_\infty = 10^6$, the asymptotic baryonic density was equal $n_\infty = 1.6 \times 10^{-19}$, and the asymptotic sound velocity was set to $a_\infty^2 = 0.1$ (here and in all other results we have adopted the gravitational units with $c = G = 1$). For such a solution the sonic point and the apparent horizon were located at $R_* = 0.82$ and $R_{\rm BH} = 0.34$ respectively, and the mass contained in the fluid constituted the bulk of the entire mass, namely $m_{\rm fluid} = 0.83$. The accretion rate for this solution reaches a very small value of $\dot{m} = 2.6 \times 10^{-18}$, thus the growth of the central object can be neglected during the entire simulation (this fact has been confirmed independently by allowing the central mass to grow according to the actual value of $\dot{m}$).

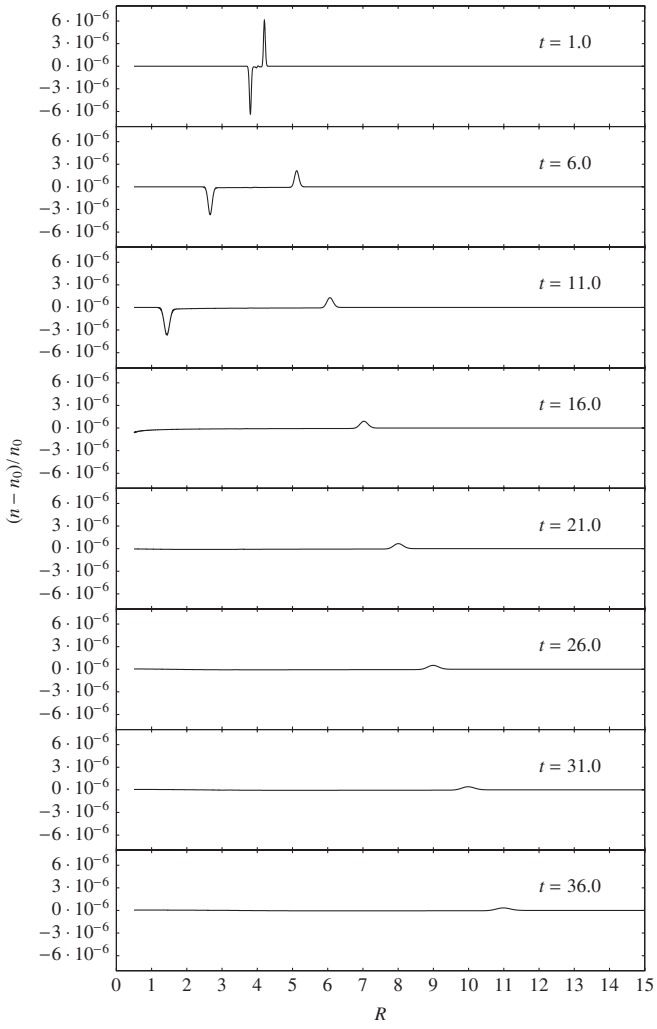

FIG. 2. Evolution of small perturbations. Here n_0 denotes the density in the unperturbed flow. The snapshots show the density contrast $(n - n_0)/n_0$ in chronological order.

VII. SONIC HORIZONS VERSUS APPARENT HORIZONS

For large initial perturbations the situation can be more complex, as will be discussed below. A discontinuous solution with shocks can develop, and we can observe some reflection of the signal that was initially propagating inwards.

Figure 3 shows snapshots from the evolution of the perturbations applied to the same background solution as before. In each of the graphs on Fig. 3 the perturbed density profile has been plotted over the profile corresponding to the steady solution. One can clearly see the stable behavior on these plots even though they are limited to the small radius range of $R < 0.5 \times 10^3$ and relatively short evolution times. The original simulations have been performed during much longer times confirming the stability of the flow. At late stages of the evolution the initial perturbation was indistinguishable from the numerical noise.

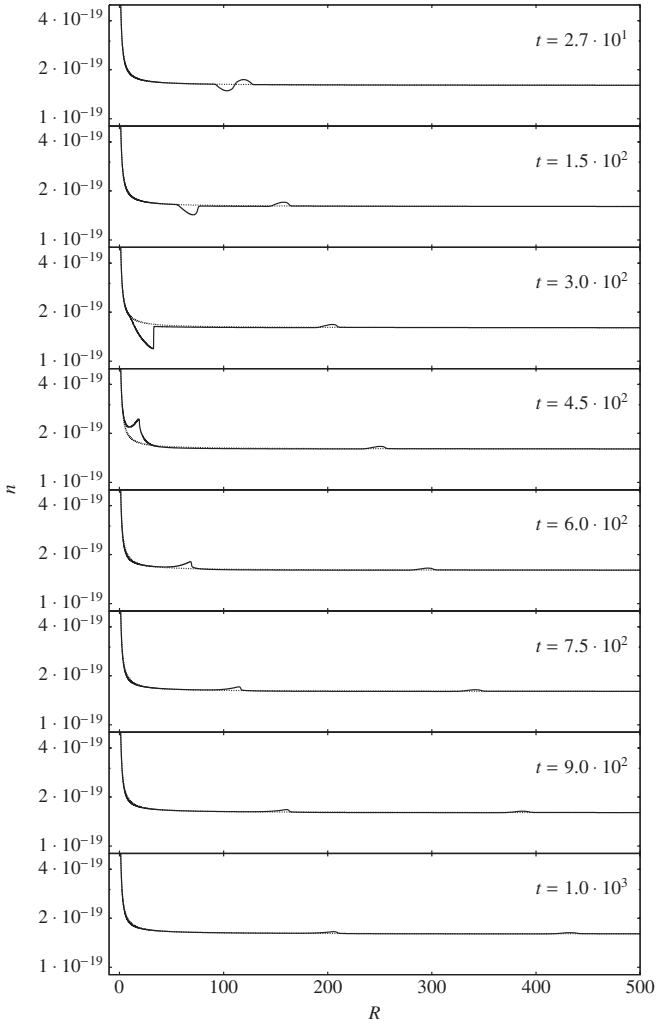

FIG. 3. Evolution of the perturbed density. The snapshots are placed in chronological order. The profile corresponding to the unperturbed flow is depicted with a dotted line.

All these numerical results suggest the stability of the accretion flow also in the regime where the mass of the fluid is large. Naturally, numerical simulations of this kind can never replace a strict mathematical proof, because we cannot investigate the whole family of possible initial data (meaning both steady solutions and perturbation profiles).

The reflection of the strong incoming signal from the inner parts of the accreting cloud is somewhat surprising. For a small and compact perturbation entering the supersonic region in the center of the cloud, it should not be possible to be reflected and reach the subsonic region again—this would require the perturbation to travel with a velocity which, relative to the unperturbed flow, should be greater than the speed of sound. Because of that fact, in analogy with the black hole horizon, the term ''sonic horizon'' has been coined to name the surface bounding the supersonic region.

A careful inspection reveals that, contrary to the event horizons surrounding black holes, this notion can only be approximate. For strong nonlinear perturbations the concept of an unperturbed background solution loses meaning. The values of the local sound speed a change due to the perturbation and new sonic points can appear. In addition, the speed of a strong shock wave is no longer limited to the local speed of sound.

Such behavior has been illustrated on Fig. 4. Here we are still dealing with the same initial solution, perturbed slightly more to show the whole phenomenon in a clearer way. The quantity Xv^R is plotted with the solid line, while for the graph of $-a$ a dotted line has been used. A part of the initial perturbation develops into the shock propagating inwards which, after some time of evolution, creates additional sonic points (i.e., intersections of graphs of Xv^R and $-a$) lying outside the original ''sonic horizon.'' When the perturbation reaches the inner parts of the cloud it even

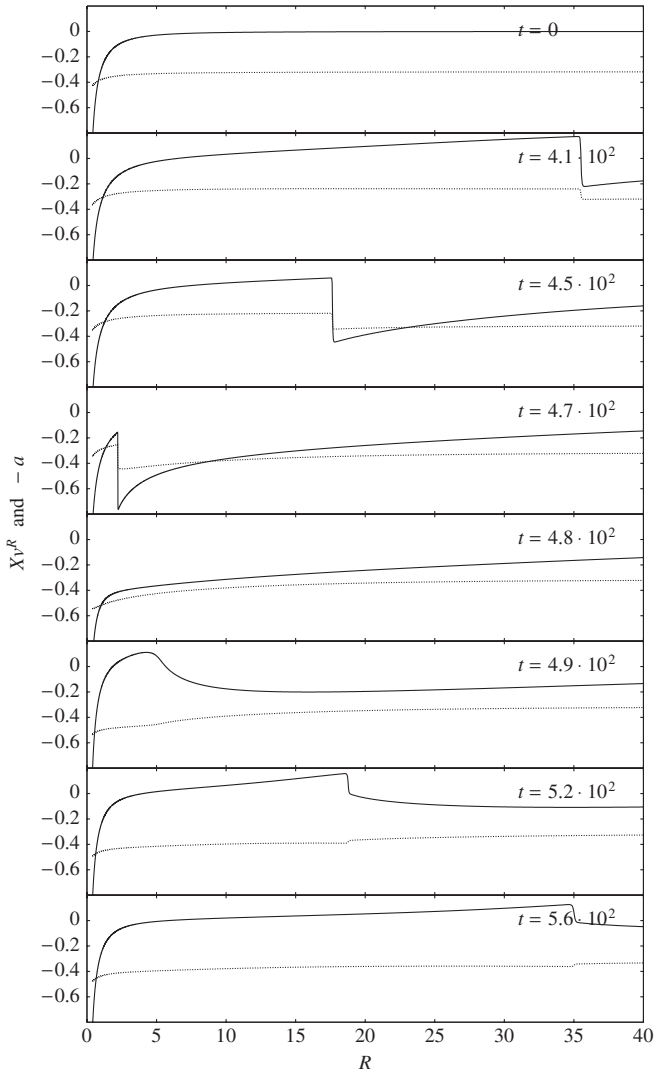

FIG. 4. Reflection of the incoming signal from the inner parts of the accretion cloud. The velocity Xv^R is drawn with the solid line, while the dotted line depicts values of $-a$. Intersections of the two graphs correspond to the sonic points (see the discussion in text).

destroys the ''original'' sonic point, which is being replaced by the newly created one. The reflected signal really becomes visible in the broad structure outside the new sonic point, or to say this differently, the outermost sonic point moves toward the center releasing the outgoing perturbation, which then propagates freely outwards.

The behavior of small perturbations of compact support confirms the standard interpretation of sonic horizons as analogs of event horizons in the linear regime. However, results concerning strong perturbations suggest that one should be careful in formulating the analogy (quite common in the so-called analogous gravity models) between the sonic horizon and the event horizon [28,29].

In summary, our numerical results reported in the last two sections suggest that in both cases—of small and large perturbations—steady accretion is stable. The amplitudes of the perturbations decrease, and after sufficient time we are left with the background solution. This can be demonstrated for both accretion regimes: solutions with a large mass in the center and having little fluid and systems with large amount of gas but possessing light compact cores.

VIII. STABILITY OF THE NEWTONIAN ACCRETION

In this section we shall report results obtained with the use of a version of the PROMETHEUS code by Fryxell, Müller, and Arnett [30], adapted to our purposes. PROMETHEUS is a Newtonian HRSC hydrodynamical code implementing the original piecewise parabolic reconstruction scheme developed by Colella and Woodward [31]. It has been extensively used for simulating such astrophysical phenomena as supernova explosions and it is capable of simulating self-gravitating flows both in spherically and axially symmetric cases. As the initial data we have used solutions to the Newtonian equations for the steady flow that include self-gravitation of the accreting fluid. An equation of state was polytropic, $p = K\rho^{\Gamma}$. A point mass m_{P} was assumed to exist at $R = 0$.

Results concerning spherically symmetric perturbations have been already presented in [32]. They are qualitatively similar to the relativistic results reported in the preceding sections. The accreting flow was stable both in the test and fluid-rich regimes. Large incoming perturbations were being reflected from the inner parts of the accretion cloud. We have also observed effects analogous to those described in the previous chapter concerning the creation and destruction of the sonic horizons. Moreover, for sufficiently small perturbations of compact support no reflection has been noticed.

Below we shall report studies of axially symmetric perturbations. In PROMETHEUS simulations of two- or three-dimensional flows are being performed using the so-called dimensional splitting. The local Riemann problems appearing in the Godunov-type method are being solved separately in each of the dimensions, but, in order to preserve consistency of the method, every time step the transversal components of velocity are also being evolved, using the effective advection equations. The subtle point about this procedure is that the order of the subsequent one dimensional sweeps is important to provide the desired accuracy of the whole scheme. This issue has been discussed in detail by Strang in [33].

The gravitational potential has to be found at each time step by solving the gravitational Poisson equation. The PROMETHEUS code implements a method, based on the expansion of the gravitational potential in terms of the spherical harmonics, that has been developed by Müller and Steinmetz [34].

In our case the Euler equations of hydrodynamics and the Poisson equation for the gravitational field were solved on a spherical grid consisting of 600 zones in the radial and 180 zones in the angular direction.

The results presented on Fig. 5 have been obtained for the following parameters of the flow. The outer boundary of the cloud was assumed to be located at $R_{\infty} = 2 \times 10^6$, the central mass was set to $m_{\mathrm{P}} = 3 \times 10^3$ (in the Newtonian limit gravitational units that we use here correspond to setting $G = 1$). As before, we have chosen a

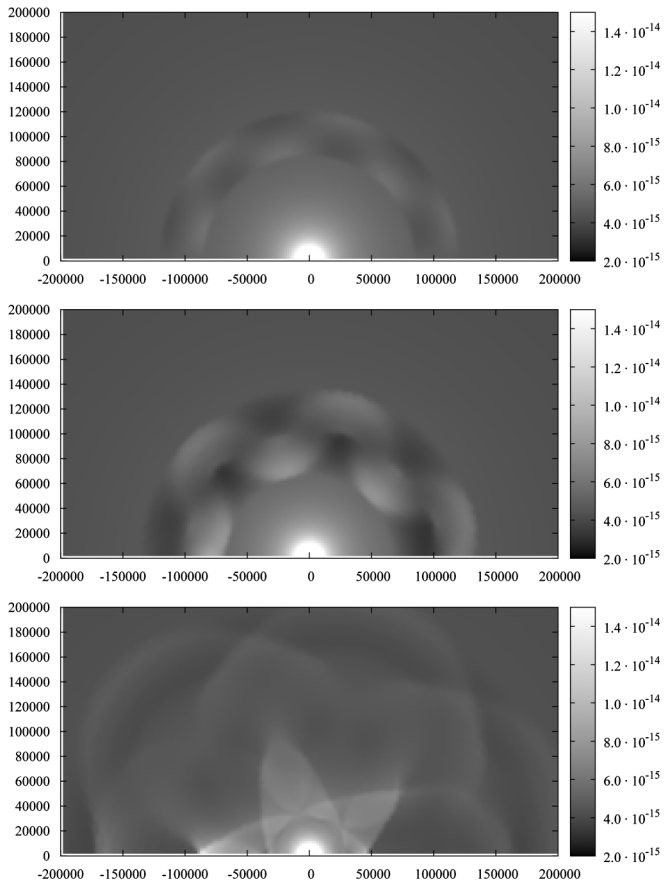

FIG. 5. Evolution of axially symmetric density perturbations of the steady accretion cloud. The plots show the spatial distribution of the density at times 5×10^3, 5×10^4, and 2.5×10^5, respectively.

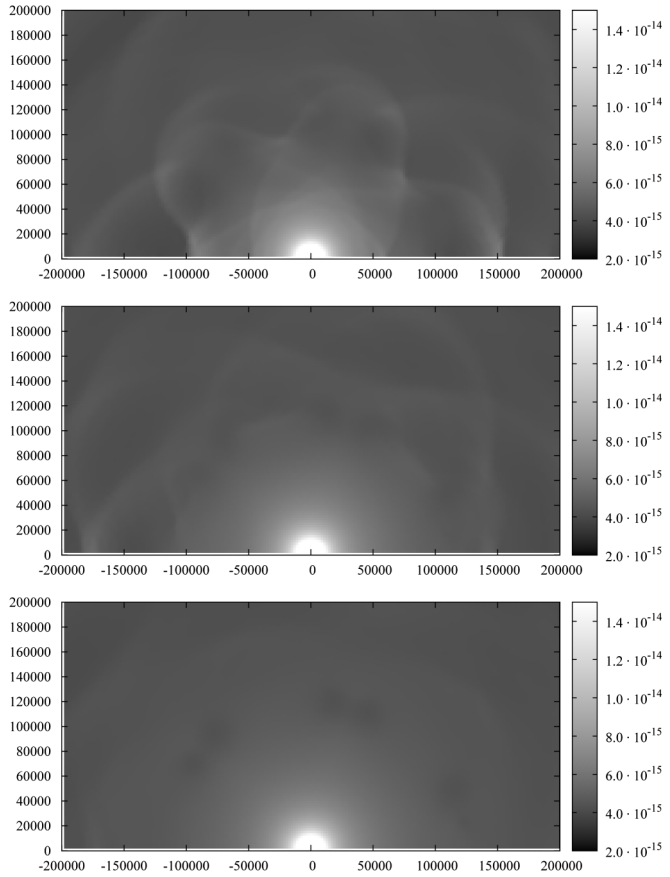

FIG. 6. Continuation of the previous figure. The subsequent snapshots correspond to evolution times of 4.5×10^5, 6.5×10^5, and 8.5×10^5, respectively.

solution where most of the mass is contained in the fluid, i.e., $m_{\mathrm{P}}/m_{\mathrm{tot}} = 3\%$. The asymptotic parameters of the unperturbed flow were as follows: $\rho_\infty = 3 \times 10^{-15}$, $U_\infty = -4 \times 10^{-5}$, and for the parameters of the polytropic equation of state we have taken $\Gamma = 1.4$, $K = 5 \times 10^4$.

Initial data coincide with the relevant characteristics of the stationary flow, with the exception of the velocity. The velocity perturbations are of the form

$$\delta U(R,\theta) = \begin{cases} A \sin(\frac{R-R_a}{R_b-R_a}\pi)\sin(6\theta) & \text{for } R_a < R < R_b, \\ 0 & \text{for } R < R_a \text{ or } R_b < R, \end{cases}$$

where A is the initial amplitude of the perturbations while R_a and R_b describe their support. This is obviously a completely arbitrary choice. The only important feature of these perturbations is their nonsphericality.

The boundary conditions have been chosen in the same way as in the relativistic case. At the inner boundary the outflow conditions were assumed, while at the outer boundary we have implemented ''external'' inflow conditions based on the background steady flow. Figures 5 and 6 show snapshots from the evolution of the density, which has been color coded using a logarithmic scale.

As expected, after a sufficient time all perturbations either disappear through the inner boundary or disperse outwards. This again suggests that the accretion flow is stable, even in the regime where the mass of the fluid dominates over that of the central object. In particular, we do not observe any fragmentation of the cloud, which might be expected in the case of nonspherical, self-gravitating accretion flows. A simple theoretical argument, basing on the unproven [35] but unreasonably effective Jeans criterion, goes as follows. The Jeans length can be estimated as $R_{\mathrm{J}} = a_\infty/\sqrt{\varrho_\infty} \approx 6 \times 10^6$. This gives a value 3 times larger than the size of the entire accreting cloud, i.e., $R_\infty = 2 \times 10^6$. That hints at the absence of a fragmentation due to self-gravity, which agrees with our numerical results. On the other hand, it is not clear whether the Jeans criterion can be applied to general nonspherical perturbations and the instability in the general case cannot be excluded.

IX. CONCLUSIONS

This paper is dedicated to the discussion of the stability of steady accretion of perfect fluids onto compact objects, with an emphasis on the self-gravitation of the accreting gas. The recently discovered steady accretion flows are rich in the fluid and the backreaction effects are important. Known analytic results do not apply to such systems. The stability investigation requires a proper handling of a set of nonlinear partial differential equations and it is accessible only by means of numerical computations. Such a numerical analysis has been performed in preceding sections using modern, high resolution and shock-capturing schemes, both in the general-relativistic case as well as in Newtonian hydrodynamics. In all examined cases the flows have been stable, even for large nonlinear perturbations. Simulations of the evolution of large, sometimes even discontinuous, perturbations have led to a remarkable observation on the so-called ''sonic horizons.'' In the linear regime, with very small perturbations, the sonic horizon can be viewed as a surface bounding a region from which no perturbation can escape; it is impenetrable from inside, analogous to the event horizons in general relativity. We show that for strong perturbations this is no longer true. Perturbations can change positions of the sonic points and easily escape from a region initially bounded by the sonic horizon. Thus, the analogy between the ''sonic horizon'' and the event horizon of a black hole is rather limited.

Our analysis of the stability is restricted to the accretion cloud only. In all numerical simulations, we had to ensure that the gas is being delivered to the system with a small, constant rate. To relax this assumption one would have to take into account a physical process that could be responsible for the feeding of the accretion cloud. One of the possibilities is to consider the so-called ''quasistars'' [10]. They consist of the spherical accretion cloud surrounded by a large, highly massive stellar envelope, being a reser-

voir of gas necessary to support the accretion. The other class of objects might constitute Thorne-Żytkow stars [8,9].

In Sec. IV we described a number of classical tests for numerical codes. Stationary accretion flows possess all essential elements—velocity field, self-gravitation, and pressure. These solutions are stable. We think that they should be included into the standard test suite for general-relativistic hydrodynamical codes.

Spherically symmetric models of accretion must be understood as a highly idealized version of physical reality. In most astrophysical scenarios, the inflowing gas is observed in the form of accretion disks deviating strongly from spherical symmetry. Nevertheless, models of spherical accretion occupy an important place in the theoretical astrophysics as elements of a more complex description of astrophysical phenomena (see, e.g., the aforementioned works on quasistars by Begelman, Rossi, and Armitage [10]). They allow for the inspection of the effects caused by self-gravity in general-relativistic hydrodynamics in a simple, but nontrivial, case.

More realistic models should take into account the radiation originated and transported through the accretion cloud. Recently, a Newtonian analysis of such processes has been published by Karkowski, Malec, and Roszkowski [27]. These works are being continued in the general-relativistic context, the results revealing the importance of self-gravity and its connection to the observational characteristics of the model such as the total luminosity of the accretion cloud or the redshift of the emitted radiation.

ACKNOWLEDGMENTS

This paper has been partially supported by the MNII Grant No. 1PO3B 01229. Numerical computations have been made at the Academic Computer Center Cyfronet, Grant No. MNiSW/SGI3700/UJ/116/2007. P. M. thanks Ewald Müller for kind agreement to use the PROMETHEUS code and for the possibility to visit the Institute of Astrophysics at Garching. The authors thank Niall Ó Murchadha for careful reading and useful comments.

[1] H. Bondi and F. Hoyle, Mon. Not. R. Astron. Soc. **104**, 273 (1944).
[2] F. Hoyle and R. A. Lyttleton, Proc. Cambridge Philos. Soc. **35**, 405 (1939).
[3] R. A. Lyttleton and F. Hoyle, The Observatory **63**, 39 (1940).
[4] H. Bondi, Mon. Not. R. Astron. Soc. **112**, 195 (1952).
[5] F. C. Michel, Astrophys. Space Sci. **15**, 153 (1972).
[6] E. Malec, Phys. Rev. D **60**, 104043 (1999).
[7] J. Karkowski, B. Kinasiewicz, P. Mach, E. Malec, and Z. Świerczyński, Phys. Rev. D **73**, 021503(R) (2006).
[8] K. S. Thorne and A. N. Żytkow, Astrophys. J. **199**, L19 (1975).
[9] K. S. Thorne and A. N. Żytkow, Astrophys. J. **212**, 832 (1977).
[10] M. C. Begelman, E. M. Rossi, and Ph. J. Armitage, Mon. Not. R. Astron. Soc. (to be published).
[11] P. Papadopoulos and J. Font, Phys. Rev. D **61**, 024015 (1999).
[12] L. Zampieri, J. C.Miller, and R. Turolla, Mon. Not. R. Astron. Soc. **281**, 1183 (1996).
[13] L. Nobili, R. Turolla, and L. Zampieri, Astrophys. J. **383**, 250 (1991).
[14] V. Moncrief, Astrophys. J. **235**, 1038 (1980).
[15] B. Kinasiewicz, P. Mach, and E. Malec, Int. J. Geom. Methods Mod. Phys. **4**, 197 (2007).
[16] J. V. Romero, J. M. Ibáñez, J. M. Martí, and J. Miralles, Astrophys. J. **462**, 839 (1996).
[17] F. Banyuls, J. A. Font, J. M. Ibáñez, J. M. Martí, and J. A. Miralles, Astrophys. J. **476**, 221 (1997).
[18] B. Van Leer, J. Comput. Phys. **32**, 101 (1979).
[19] R. Donat and A. Maraquina, J. Comput. Phys. **125**, 42 (1996).
[20] M. A. Aloy, J. M. Ibáñez, J. M. Martí, and E. Müller, Astrophys. J. Suppl. Ser. **122**, 151 (1999).
[21] E. Gourgoulhon, Astron. Astrophys. **252**, 651 (1991).
[22] R. D. Blandford and C. F. McKee, Phys. Fluids **19**, 1130 (1976).
[23] R. F. Tooper, Astrophys. J. **142**, 1541 (1965).
[24] E. Hairer, S. P. Norsett, and G. Wanner, *Solving ordinary differential equations I. Nonstiff problems*, Springer Series in Computational Mathematics (Springer–Verlag, Berlin, 1993).
[25] P. N. Brown, A. C. Hindmarsh, and L. R. Petzold, SIAM J. Sci. Comput. **15**, 1467 (1994).
[26] S. Li and L. R. Petzold, *Design of new DASPK for sensivity analysis*, Technical Raport, University of California Santa Barbara, Santa Barbara, 1999.
[27] J. Karkowski, E. Malec, and K. Roszkowski, Astron. Astrophys. **479** (1), 161 (2008).
[28] T. K. Das, Classical Quantum Gravity **21**, 5253 (2004).
[29] S. Dasgupta, N. Bilić, and T. K. Das, Gen. Relativ. Gravit. **37**, 1877 (2005).
[30] B. A Fryxell, E. Müller, and W. D. Arnett, Max-Planck-Institut für Astrophysik, Garching, Report No. 449, 1989.
[31] Ph. Colella and P. R. Woodward, J. Comput. Phys. **54**, 174 (1984).
[32] P. Mach, Acta Phys. Pol. B **38**, 3935 (2007).
[33] G. Strang, SIAM J. Numer. Anal. **5**, 506 (1968).
[34] E. Müller and M. Steinmetz, Comput. Phys. Commun. **89**, 45 (1995).
[35] W. B. Bonnor, Mon. Not. R. Astron. Soc. **117**, 104 (1957).